Atmos. Chem. Phys. Discuss., 15, 27177–27218, 2015
www.atmos-chem-phys-discuss.net/15/27177/2015/
doi:10.5194/acpd-15-27177-2015

Atmospheric Chemistry and Physics Discussions
Open Access

Atmospheric salt deposition in a tropical mountain rain forest at the eastern Andean slopes of South Ecuador – Pacific or Atlantic origin?

S. Makowski Giannoni[1], **K. Trachte**[1], **R. Rollenbeck**[1], **L. Lehnert**[1], **J. Fuchs**[2], and **J. Bendix**[1]

[1]Laboratory for Climatology and Remote Sensing (LCRS), Institue of Physical Geography, Department of Geography, Philipps-Universitaet, Marburg, Germany
[2]Laboratory of Climatology, Institute of Physical Geography, Department of Geography, Ruhr-Universitaet, Bochum, Germany

Received: 17 June 2015 – Accepted: 17 September 2015 – Published: 8 October 2015

Correspondence to: S. Makowski Giannoni (sandro.makowski@posteo.org)

Published by Copernicus Publications on behalf of the European Geosciences Union.

Abstract

Salt (NaCl) is recently proven to be of highest importance for ecosystem functioning of the Amazon lowland forests because of its importance for herbivory, litter decomposition and thus, carbon cycling. Salt deposition should generally decline with distance from its marine sources. For tropical South America, a negative east-west salt availability gradient is assumed in the Amazon as a consequence of the barrier effect of the Andes for Pacific air masses. However, this generalized pattern may not hold for the tropical mountain rain forest in the Andes of southern Ecuador. To analyze salt availability, we investigate the deposition of Na^+ and Cl^- which are good proxies of sea spray aerosol. Because of the complexity of the terrain and related cloud and rain formation processes, salt deposition was analyzed from both, rain and occult precipitation (OP) water along an altitudinal gradient over a period from 2004 to 2009. To assess the influence of Atlantic and Pacific air masses on the locally observed deposition of sodium and chloride, sea-salt aerosol concentration data from the Monitoring Atmospheric Composition and Climate (MACC) reanalysis dataset and back-trajectory statistical methods were combined. Our results based on deposition time series and 2192 generated trajectories show a clear difference in the temporal variation of sodium and chloride concentration due to height and exposure to winds. The sea-salt transport was highly seasonal where higher locations revealed a stronger seasonality. Although the influence of the easterlies were predominant regarding atmospheric circulation, the statistical analysis of trajectories and hybrid receptor models revealed a stronger impact of the Pacific sea-salt sources on the deposition at the study area. The highest concentration in rain and cloud water was found between September and February originating from both, the equatorial Pacific and Atlantic. However, the Pacific sources contributed with up to 25 % to the observed total concentration of Na^+ and Cl^- at the receptor site although the frequency of occurrence of the respective trajectories is below 10 %. This highlights the great importance of westerly winds from the Pacific for

ACPD

15, 27177–27218, 2015

Atmospheric deposition of sea-salt in South-eastern Ecuador

S. Makowski Giannoni et al.

the sea-salt transport to the deposition into the tropical mountain forests at the eastern Andean slopes of southern Ecuador.

1 Introduction

Poor substrate and intense leaching by precipitation make tropical forests particularly prone to nutrient limitation. While phosphorus is mainly claimed to limit net primary productivity (NPP) in lowland Amazonian tropical forest, phosphorus and nitrogen co-limits growth in the tropical montain rain forests as e.g in southern Ecuador (Homeier et al., 2012; Koehler et al., 2009; Tanner et al., 1998; Vitousek, 1984; Wolf et al., 2011; Wullaert et al., 2010). Because of a world wide increase in nitrogen and phosphorus emissions and a particularly accelerated enhancement of emissions in developing countries, where most of the tropical forests are located, atmospheric deposition in these countries has gained some attention (Dentener et al., 2006; Galloway et al., 2008; Phoenix et al., 2006).

Nitrogen and phosphorus cycling and deposition from atmospheric sources are been investigated in several tropical and temperate forests, where the changes in the nitrogen and phosphorus budgets are expected to have impacts in ecosystem structure and functioning and plant diversity (Bobbink et al., 2010; Brookshire et al., 2012; Homeier et al., 2012; Matson et al., 2014; Pett-Ridge, 2009; Phoenix et al., 2006; Wang et al., 2014; Wilcke et al., 2013; Yu et al., 2015). The role of salt availability has very recently gained attention as it has been found to condition the behaviour of herbivores, as well as affecting carbon cycling and organic matter decomposition in tropical ecosystems (Dudley et al., 2012; Kaspari et al., 2008, 2009; Powell et al., 2009; Voigt et al., 2008). In spite of its pantropical importance it has been hitherto overlooked in most biogeography and biogeochemistry studies (Dudley et al., 2012).

By far, the most important source of continental salt depositions are the oceans. In the Amazon, shielded by the natural orographic barrier of the Andes, to the West, salt scarcity in rain water increases along a gradient from the Atlantic coast towards the

ACPD
15, 27177–27218, 2015

eastern declivity of the Andes. Both, Na^+ and Cl^- concentration in rain water diminished significantly with distance from the Atlantic Ocean. Additionally, the ratio between both concentrations inverts from $Cl^- > Na^+$ close the ocean to $Cl^- < Na^+$ far from the ocean (Tardy et al., 2005). Consequently, tropical mountain forests on the Andes eastern slopes and tropical lowland forest at the western edge of the Amazon are expected to suffer from salt deprivation, as opposed to forests closer to the Atlantic coast, where salt deposition is large (Dudley et al., 2012). Particularly in the former, there is evidence that herbivore and frugivore birds and mammals visit mineral licks to compensate for low sodium concentration in plant and fruit tissues in the Amazon of Peru, Ecuador, and Colombia (Lee et al., 2009; Lizcano and Cavelier, 2004; Powell et al., 2009; Voigt et al., 2008). Some arthropod taxa in the West Amazon have also been reported to practice geophagy to deal with salt scarcity in plants (Kaspari et al., 2008).

The tropical mountain forests at the eastern Andean slopes in southern Ecuador may likely represent an exception of this generalized pattern because of their location in the Huancabamba depression, an area where the Andes rarely exceed altitudes > 3600 m, which might represent a better connection to the Pacific salt sources. In consequence, the mountain forest might benefit not only from salt transported by easterly air masses from the Atlantic but also by salt originating from Pacific air masses. Depending on the strength of the contribution to sodium deposition from Pacific, the combined sodium input from Atlantic and Pacific sources could result in a greater salt availability than that found for the lowland forests in the western rim of the Amazon (Dudley et al., 2012).

However, only few research has been conducted to investigate the deposition of atmospheric sodium and chloride in the tropical forests of the South-Ecuadorian Andes and to identify their sources. An exception is the work of Fabian et al. (2009) who estimated the origin of salt deposited aerosols by visual interpretation of single back-trajectories. To our knowledge, no comprehensive quantitative investigation on salt sources nor any estimations of their contribution to the atmospheric deposition have been conducted yet.

ACPD
15, 27177–27218, 2015

As a consequence of the knowledge gaps regarding the salt sources of deposition in the Andes of south-eastern Ecuador, the aims of the present study are (1) to characterize sodium and chloride atmospheric deposition by rain and occult precipitation along an altitudinal gradient and at different topographical locations in a tropical mountain rain forest site, (2) to allocate potential geographical sources in the Pacific and Atlantic oceans applying potential source contribution function (PSCF) and concentration weighted trajectory (CWT) analysis, and (3) to estimate the contribution of each source area to the deposition of sodium and chloride in our study area.

2 Study area

The study area is located at the north-western edge of the Amazon basin (4°00′ S, 79°05′ W), at the southeastern Andes of Ecuador, approx. 100 km straight line distance away from the Pacific coast and around 2000 km from the closest part of the Atlantic coast. The central study area comprises the Rio San Francisco valley, deeply incised into the eastern slope of the main Andes Cordillera. Since 2002, the Reserva Biologica San Francisco (RBSF), located on the northern slopes of the valley and some areas outside of the reserve have been the subject of investigations from two successive multidisciplinary research programs (Beck et al., 2008; Bendix et al., 2013).

The Andes in this area are characterized by lower elevations and a highly geomorphological complexity compared to other parts of the mountain chain in northern Ecuador, Peru, and Colombia. Because it is proven that exposure and altitude affects deposition (Griffith et al., 2015; Kirchner et al., 2014; Lovett and Kinsman, 1990; Makowski Giannoni et al., 2013) the current investigation along a large altitudinal gradient and at different slope exposures is the precondition to unveil salt deposition. The valley of San Francisco facilitates such a study design because of its rough terrain.

The climate of the catchment is mainly determined by the activity of the constant easterly trade winds from north and south-east, being those from the north-east dominant. However, because of the low altitude of the mountains when the trade winds

ACPD
15, 27177–27218, 2015

weaken at the end and beginning of each year, westerly wind bursts occur, carrying with them Pacific air masses (see Fig. 1) (Bendix et al., 2008a; Emck, 2007). Precipitation responds to the migration of intertropical convergence zone (ITCZ) and the dynamics of the easterly trades. The season of highest rainfall occurs between June and August, when the easterly winds predominate, carrying masses of humid air from the lowlands of the Amazon. The topography forces the humid air to move upwards leading to high rainfall sums especially in the higher parts of the mountains and facilitates the immersion of peaks into clouds resulting in occult precipitation (OP; Bendix et al., 2006, 2008b; Richter et al., 2013; Rollenbeck et al., 2011). The average rainfall varies between 1500 and 6500 mm per year between 1960 and 3180 m for the period 2004 to 2009. In the highest parts OP contributes to up to 35 % of total precipitation (Rollenbeck et al., 2011). A short dry season occurs between November and March where Pacific air masses are transported with occasional westerlies to the area with frequencies less than 20 % of the time (Richter et al., 2013) and accompanied with thunderstorms and convective activity.

3 Data and methods

The methodology we used is divided into two main parts: The analysis of the concentration of sodium and chloride in rain and OP samples, and the allocation of potential sources of salt by a method that combines air-mass back-trajectories and reanalysis data of sea-salt concentration in the atmosphere. Because of the complexity of the terrain, in the first part we assessed the levels of sodium and chloride concentration in samples of rain and OP from different meteorological stations (MSs) along an altitudinal gradient, as well as the temporal variation in the concentration at each elevation. To make a first evaluation of the possible origin of sodium and chloride we have also analyzed its relationship to the other ions analyzed using a principal factor analysis. The second part focuses on the description of the general atmospheric circulation patterns, the detection of potential sources of salt, and their contribution to the transport of salt

ACPD
15, 27177–27218, 2015

to our study area. As done for the concentration data from MSs, the temporal variation of air-mass transport and source contribution was accounted for by assessing its seasonal patterns. The next sections deepen into the materials and methods outlined in this introductory paragraph.

3.1 Sample collection and materials

Three MSs have been installed on the north-facing slopes of the Rio San Francisco valley along an altitudinal transect ranging from 1960 to 3180 m. A fourth station (El Tiro, 2725 m) was installed about four kilometers up-valley at a mountain pass on the Cordillera Real (Fig. 1).

Regular rain and OP sampling has been carried out at all stations from 2004 to 2009. While rain water is collected in conventional totalling gauges (UMS 200; made of Polyethylen to warrant chemical inertia), occult precipitation is collected by 1 m^2 mesh grid fog collectors following the design proposed by Schemenauer and Cereceda (1994). Details about rain and fog measurement techniques, calibration and data handling are described in Rollenbeck et al. (2007) and Rollenbeck et al. (2011). Rain and OP samples were collected in almost regular weekly intervals. The samples were filtered and stored in frozen state immediately, before being sent to the laboratory for ion analyses.

All samples were analysed at the University of Munich's Weihenstephan center (TUM-WZW) for major ions (K^+, Na^+, ${NH_4}^+$,Ca^{2+},Mg^{2+}, Cl^-, ${SO_4}^{2-}$, ${NO_3}^-$, ${PO_4}^{3-}$). Cation analyses were carried out by the inductivity-coupled plasma method (Perkin Elmer Optima 3000), while anions were analyzed by ion chromatography (Dionex DX-210). Since sea spray aerosol consists mainly of chloride and sodium (Millero, 2014), we found adequate to use the concentration of Na^+ and Cl^- in rain and OP as proxies of sea-salt atmospheric inputs into the ecosystem. Being a conservative ion in sea-salt aerosol, Na^+ has been often used as reference for sea-salt concentration in precipitation chemistry and atmospheric chemistry modeling studies (Jaeglé et al., 2011; Keene et al., 1986; Pozzer et al., 2012; Tardy et al., 2005; Vet et al., 2014).

ACPD
15, 27177–27218, 2015

Weekly Na^+ and Cl^- concentration in water samples from rain and OP was weighted with the total weekly precipitation volume, averaged to monthly means of volume weighted concentration (VWMM). With the calculated VWMM we compiled monthly time-series of salt concentration for a 6 year time series from 2006 to 2009. Additionally we computed total volume weighted means (VWM) to compare our observations with those from other studies. To check for differences in salt concentration between the sites located at different altitudes we computed box plots of total concentration at each altitudinal level.

Finally, factor analysis was applied to all measured ion species to look for common transport histories. Before factor analysis was conducted, the data was normalized and scaled to gain comparable distributions. For sea-salt concentration in the atmosphere we used the sea-salt mixing ratio of the Monitoring Atmospheric Composition and Climate (MACC) reanalysis data set as proxy. The concentration of sea-salt generated by wind stress on the ocean surface are diagnosed based on a source function by Guelle et al. (2001) and Schulz et al. (2004) accounting for sedimentation, and wet and dry deposition processes. In this function wet sea-salt mass fluxes at 80 % relative humidity are integrated for the three size bins (0.03 to 0.5, 0.5 to 5.0, and 5.0 to 20.0 microns) and sea-salt concentration is calculated for 60 model levels with the model top at 0.1 hPa (Morcrette et al., 2009).

3.2 Back-trajectory and source-receptor analysis

Ten days long back-trajectories of air masses were generated with the HYSPLIT model (Draxler and Hess, 1998) using the openair R package (Carslaw and Ropkins, 2012). The wind fields are represented by NCEP/NCAR reanalysis (Kalnay et al., 1996) with a grid resolution of 2.5° by 2.5°. All trajectories had their origins at the ground measurement sites from El Tiro and Cerro del Consuelo in South-Ecuador. The MACC sea-salt concentration data set was set as proxy of sea-salt concentration in the atmosphere for air-mass transport analysis by back-trajectory modeling.

ACPD
15, 27177–27218, 2015

Cluster analysis was applied to the back-trajectories to group similar air mass histories and to post process concentration data in relation to cluster origin. Euclidean distance was used as measure of similarity between different trajectories. In a next step we calculated the frequency of trajectories represented by each cluster to analyze the sea-salt concentration in relation to each of them. Furthermore, we compared the contribution of each cluster to the concentration in the monthly MACC reanalysis sea-salt concentration time-series. The choice of monthly time-series is justified because it permits the post-comparison with the Na^+ and Cl^- measured concentrations.

As stated in the objectives, our main goal is to identify the potential geographical origin of high sea-salt concentration at the receptor site in the RBSF. For this particular purpose we used source-receptor modeling as it has been successfully applied to determine likely geographical origins of pollutants and aerosols (e.g., Fleming et al., 2012; Hsu et al., 2003; Powell et al., 2009; Riuttanen et al., 2013; Robinson et al., 2011). Here, two different hybrid receptor models for comparison were used: the PSCF and the adjusted CWT running on a grid that covers the domain of the 2192 generated trajectories between 2004 and 2009. The PSCF (Pekney et al., 2006; Zeng and Hopke, 1989) calculates the probability that a source of aerosol or pollutant observed at the ground measurement site is located at a specific cell in the geographical space and is defined by:

$$\mathrm{PSCF}_{ij} = \frac{m_{ij}}{n_{ij}} \tag{1}$$

where n_{ij} is the number of trajectory points that passed through cell (i, j) and m_{ij} is the number of times that trajectory points passing through the cell (i, j) correspond to high concentration values (above an arbitrary threshold) at the time of arrival of the trajectory to the receptor site. The function is based on the premise that, if a source is located at that specific location, the air masses represented by the trajectory passing through the collocated cell are likely to collect and transport the material along the trajectory until the receptor site. In this study, we defined two concentration thresholds: the 75th percentile for moderate-to-high concentration and the 90th percentile for only high concentration.

The adjusted CWT function uses a grid domain to calculate a grid-wise logarithmic mean concentration of an aerosol or pollutant (Seibert et al., 1994) and is defined by:

$$\ln\left(\overline{C}_{ij}\right) = \frac{1}{\sum\limits_{k=1}^{N} t_{ij}} \sum_{k=1}^{N} \ln\left(\overline{C}_k\right) t_{ijk} \quad (2)$$

where i and j are the grid indices, k the trajectory index, N the total number of trajectories, $\overline{C}_k$ the pollutant concentration measured upon arrival of trajectory k, and t_{ijk} the residence time of trajectory k in grid cell (i, j). In this method, a weighted concentration is assigned to each pixel in the domain. This concentration is the average of the sample concentration at receptor that have associated trajectories crossing the respective cell.

4 Results

4.1 Sodium and chloride concentration

Since our study area is characterized by the intricated topography of the Andes (see Fig. 1), we first examined the temporal variation and distribution of the sodium and chloride concentrations in rain and OP from MSs at different altitudes and topographical locations.

Figure 2 (left column) depicts the time-series of Na^+ and Cl^- concentration from MSs at different altitudes. Cerro del Consuelo meteorological station (MS), situated at 3180 m altitude, presents the clearest temporal pattern in the concentration of salts, where the highest peaks take place almost regularly between September and February

(Fig. 2a). For Na^+ the highest peaks are found in the MSs of El Tiro (2825 m) and Cerro del Consuelo (Fig. 2a and d). Opposed to this, Cl^- concentration peaks in OP are highest at the lowermost MS, ECSF (Fig. 2c). To compare the respective distributions, the boxplots in Fig. 2 (right column) show the concentration of sodium and chloride for both, rain and OP for each considered MS. Overall, no essential variations between the concentration at each MS can be observed except for Cl^- in OP water at ECSF MS (Fig. 2d), that presented values much higher than those measured at other elevations. Regarding ion concentration in sodium and chloride species a clear difference can be observed with Cl^- concentration in the interquartile range extending between 0.22 and 0.51 mg L^{-1}, and Na^+ concentration extending between 0.06 and 0.20 mg L^{-1}.

In the rain samples, Cl^- concentration is considerably higher than the Na^+ concentration at all MSs. A larger spread and higher extreme values are observed in Cl^- concentration. Na^+ concentration do not present a relevant difference between MSs at different altitudes. The concentration show a little increase at TS1 MS (median of 0.14 mg L^{-1}) and El Tiro (median of 0.13 mg L^{-1}) and decreases again at the highest station Cerro del Consuelo (median of 0.07 mg L^{-1}).

Compared to the rain samples, OP contains a higher mean Na^+ and Cl^- concentration but also a larger spread in its distribution (Fig. 2, left column). The concentration of Cl^- is also significantly higher than that of Na^+, with highest mean concentration (median of 0.62 mg L^{-1}) at the lowest MS of ECSF. The concentration of Na^+ peaks at El Tiro MS (0.17 mg L^{-1}). At TS1 MS, the mean concentration is lowest (median of 0.09 mg L^{-1} for Na^+ and 0.3 mg L^{-1} for Cl^-), increasing once again at the highest elevations, El Tiro and Cerro del Consuelo (median between 0.11 and 0.17 mg L^{-1} for Na^+ and between 0.33 and 0.35 mg L^{-1} for Cl^-). To gain some insights on the origin of salt inputs, a factor analysis of all analyzed major ion concentration from the MSs was conducted. The analysis indicates four components which explain most of the variability in the dataset. Na^+ and Cl^- have large loadings on factors 1 or 2, depending on the MS's altitude and location, and the precipitation type. This two factors explain at least 29 % of the variability in the system (Fig. 3). With the exception of the lowermost station

ACPD
15, 27177–27218, 2015

Atmospheric deposition of sea-salt in South-eastern Ecuador

S. Makowski Giannoni et al.

(ECSF, 1960 m), Na^+ and Cl^- explain the greatest variability in the system, in the rain samples. The ECSF station, as shown in Fig. 2, presents a different distribution in the chloride concentration than that from MSs at higher elevations.

At Cerro del Consuelo MS, compounds from biomass burning co-dominate the variability in rain, given that SO_4^-, NO_3^-, Na^+, and Cl^- load to factor 1 (Fig. 3a). This means that Na^+ and Cl^- share a common air mass history with NO_3^- and SO_4^- and thus, the salt concentration has most likely an Atlantic origin. In OP samples, the biomass-burning compounds have a stronger signal, loading to factor 1. Factor 2 represents sea-salt sources only, since solely Na^+ and Cl^- load to factor 2. The origin is most probably the sporadic intrusion from Pacific air masses. At El Tiro MS, factor 1 in rain and factor 2 in OP represent sea-salt sources only (Fig. 3b). Sea-salt represents the most important factor in rain and the second most important in OP, behind biomass burning sources from the Amazon. The situation at TS1 is not so clear compared to Cerro del Consuelo and El Tiro MSs, given the combined influence of the local valley-mountain wind system and the synoptic system. In rain, Na^+ and Cl^- are dominating the variability, as they present high loadings on factor 1 (Fig. 3c). In OP, they continue to show high loadings on factor 1, but this time they share a transport history with NO_3^- and SO_4^-. In the OP samples at ECSF MS, Na^+ and Cl^- load to factor 1 together with Ca^+ and Mg^+ (Fig. 3d). In the rain samples Ca^+ and Mg^+ dominate the variability loading to factor 1, while Na^+ and K^+ load to factor 2. Cl^- does not play any role in this type of precipitation.

4.2 General transport pathways and spatial allocation of sources

In the last section we analysed the temporal and altitudinal concentration of Na^+ and Cl^- concentrations in the deposition through rain and OP, and related them to the other ions measured in deposited rain and OP water. The remaining question of where the Na^+ and Cl^- source areas are located geographically is elaborated in this subsection. To spatially locate the sources we used HYSPLIT back-trajectories and MACC sea-salt

ACPD
15, 27177–27218, 2015

concentration. Based on a correlation analysis between Na^+ and Cl^- concentrations in rain and OP measured at the two uppermost MSs (El Tiro and Cerro del Consuelo) and the reanalysis sea-salt concentrations for three size bins at six common pressure levels (see Table A1) three different target altitudes were selected: 3180 m which is the altitude of the highest MS Cerro del Consuelo and already infringes the lower tropospheric layer, as well as two other target altitudes that penetrate deeper into the synoptic layer (4200 and 6000 m). We chose the MACC dataset at 700 hPa pressure level and the medium particle size (0.5–5.0 micrometers) as input parameter for the backward trajectory analysis because it yielded the highest correlation coefficient and significance level. That being so, it demonstrated to best represent the conditions observed at the ground measurement site.

Trajectory cluster analysis was applied to identify the main representative air mass transport patterns, and so the transport pathways of sea-salt (Figs. 4, 5 and 6). As shown in panel (a) of Figs. 4–6 the easterly winds are dominant at all tested target altitudes. For the lower height levels (panel a in Figs. 5 and 6) the clustering results were very similar, where predominantly fast flowing east trajectories characterize the air mass transport (from approximately 87 to 90 % of the trajectories), and less frequent slower moving trajectories from the west (between approximately 9 and 10 %) appear rather sporadically. At 6000 m height level the air flow speed increases in both, easterly (approximately 92 %) and westerly (approximately 8 %) trajectories (Fig. 4a). The latter lose its vortex-like sweep as in Figs.5a and 6a, as a result of a decreasing influence of the transport of air masses along the Peruvian coast. In Fig. 4a, only cluster six (C6) originates in the Equatorial Pacific, while cluster four (C4) moves to the north. Cluster three (C3) originates east of the RBSF, flows across the Andes and over the Pacific and turns back towards the east to finally reach the receptor site. This type of bow-shaped trajectories is common to all three target altitudes (Fig. 4a, C3; Fig. 5a, C4 and C6; and Fig. 6a, C3, C4, and C5) and characterizes the coastal wind system associated with the Humboldt current (Bendix et al., 2008a; Emck, 2007).

ACPD
15, 27177–27218, 2015

The mean sea-salt concentration for the trajectory clusters arriving at the RBSF is presented in Table 1. The Pacific clusters (Table 1 C3, C4, C5 for 3180 m, C4, C5, C6 for 4200 m, and C3, C4, C6 for 6000 m) reveal a higher concentration of sea-salt, whereas easterly air passing over the Atlantic and the South American continent before arriving at the RBSF show intermediate to lower concentrations. North-easterly trajectories for example were associated with an intermediate concentration, while easterlies and south-easterlies had only small concentrations related to them. In addition to the cluster-associated mean NaCl sea-salt concentration it is also valuable to know in which proportion each cluster adds to the total concentration in the analyzed study period. The values in parenthesis in Table 1 summarize the contribution in percentage of each cluster. For the trajectories arriving at 3180 and 4200 m height level (Table 1) cluster C1, representing the north-easterlies, had the highest contributions. Furthermore, once added the contribution from the other two easterly clusters (Table1 C2 and C6 for 3180 m, C2 and C3 for 4200 m, and C2 and C5 for 6000 m), approximately 74 to 80 % of the total concentration is associated with an easterly transport of air masses coming from the Atlantic. The remaining 20 to 25 % are attributed to air flows passing over the Pacific before reaching the RBSF. These highly loaded seasonal Pacific flow incursions take place in the southern hemisphere's late-spring and summer as easterlies weaken due to the south-ward shift of the ITCZ. This pattern is clearly shown in panel b of Figs. 4–6, where sea-salt time-series describe the proportion of concentration contributed by each cluster. Atlantic air masses add to the concentration constantly along the year, also in winter, when the Pacific flows does not play any role. However, the high peaks at the end and the beginning of each year are clearly dominated by the transport from the Pacific. The same seasonal patterns were also identified in the measurements in Fig. 2, being clearest at the highest station Cerro del Consuelo (Fig. 2a), which means that it is possible to explain the observed patterns in the measurements by the large-scale atmospheric circulation patterns.

After characterizing the main pathways of air masses on the basis of back-trajectories and cluster analysis, we take a look at potential sources which might con-

ACPD
15, 27177–27218, 2015

tribute to the sea-salt concentration at the receptor site. For this reason two hybrid receptor models were used as shown in Fig. 7. In order to capture source areas responsible of moderate and high concentration contributions at the receptor site we applied the PSCF with two distinct predefined concentration thresholds, the 75th and the 90th percentiles, and the CWT function, which inherently discriminates between sources of moderate and high intensity. In accordance with the back-trajectories these functions were applied for three selected height levels of 6000, 4200, and 3180 m (Fig. 7).

When we compare the spatial distribution of potential sea-salt sources between the two models (PSCF and CWT) similar locations in the Atlantic and Pacific Oceans can be observed. The highest probabilities/concentration (above 0.5 for Fig. 7a–f and above $5e^{-9}$ for Fig. 7g–h) occur in the equatorial Pacific, which points to stronger sources of sea-salt in that region contributing to the high concentration at the receptor site and confirms the results of the trajectory cluster analysis in Table 1. The target altitudes of the back-trajectories (left, middle and right columns in Fig. 7) show a generally coinciding location of source transport pathways. However, at the lowest target altitude (Fig. 7, right column) the transport along the coast of Peru becomes more important due to the increasing influence of the lower tropospheric wind system. High sea-salt emission sources are expected to be found whether in the Pacific or in the Atlantic. To judge from the high probabilities/concentration over the oceans, the PSCF with 90th percentile threshold (Fig. 7d, e, f) and the CWT (Fig. 7g, h, i) performed best in discriminating between potential geographical sources that contribute to moderate and high sea-salt concentration at RBSF in South Ecuador. In contrast, the PSCF with 75th percentile threshold (Fig. 7a, b, c) only detected the transport pathways for sea-salt irrespective of the intensity of the source contribution to the concentration.

4.3 Seasonal patterns in sea-salt transport and source contribution

The synoptic wind system over South America is driven by strong seasonal circulation patterns. Because the air mass transport until the receptor site is directly linked to the seasonal cycle of the large-scale circulation system (Bendix et al., 2008a; Emck,

ACPD
15, 27177–27218, 2015

2007) and thus, sources of sea-salt concentration and their intensity may vary with seasons we examined if seasonal patterns are present in the dominant clusters for each height level. For this reason the sea-salt concentrations related to each clusters were separated by months and years to get an overview on its temporal variations.

Figure 8 illustrates the mean sea-salt concentration for each cluster and the three distinct height levels analyzed. Based on the highest values in austral late spring (SON) and summer (DJF), when mean concentration are frequently above 8–9 $\mathrm{kg\,kg^{-1}}$, it is evident that the highest mean sea-salt concentration is related to the westerly and north-easterly air masses. During this time the western and north-eastern clusters also present a more or less strong seasonality (lusters C3, C4, C5 and C6 in Fig. 8a; clusters C1, C4, C5 and C6 in Fig. 8b, and clusters C1, C3, C4 and C5 in Fig. 8c) owing to the fact that westerlies are only present during SON and DJF, while north-easterlies are absent during the austral winter (JJA) following the migration of the ITCZ to the north. The eastern and south-eastern clusters exhibit no seasonal pattern, because they are the prevailing wind directions throughout the year. The sea-salt concentration associated with these clusters is much weaker, but due to its high frequency it contributes more continuously to the transport of background concentration from the Atlantic.

Again, to look for seasonality in the location of potential sources we calculated seasonal PSCF and CWT maps. Figures 9 and 10 show the spatial distribution of potential sources for the PSCF (90th percentile) and the CWT for DJF, MAM, JJA, and SON at the 3180 m receptor height level only. The two remaining height levels at receptor site are not shown because they give no further information. The sources that have the greatest impact, i.e. responsible for the high sea-salt concentrations at receptor site, occur between September and February (DJF and SON). During SON the source on the equatorial Pacific is dominant, while in DJF both Pacific and Atlantic sources contribute to the concentration. Yet, the Pacific sources still appear stronger, as indicated by the high concentration of pixel with high probability values in that area. On the other hand, during austral autumn (MAM) and winter (JJA) no relevant potential sources of high sea-salt concentration were identified by the models.

ACPD
15, 27177–27218, 2015

5 Discussion

In this study we examined potential sources of Na^+ and Cl^- observed in rain and OP along an altitudinal gradient in the south-eastern escarpment of the Ecuadorian Andes. The analyses were carried out by back-trajectory statistical analysis and two source-receptor models. Owing to the rough terrain, we first explored the distribution of sodium and chloride inputs by rain and OP measured in the study area in dependence of the altitude and thus, its wind exposure. Overall, comparisons between the MSs revealed a difference in the temporal variation of the concentration of Na^+ and Cl^- in rain and OP depending on the elevation and exposure. Moreover, the highest MS Cerro del Consuelo described a distinct seasonal pattern, lacking or less accentuated for the remaining MSs. The largest concentration in deposited water occurred between September and February, concomitantly with the southward migration of the ITCZ and the more frequently occurring north-easterly winds (see Fig. 2). Regarding the total concentration, Cl^- was always considerably higher than Na^+, which agrees with findings by Tardy et al. (2005). In their study, they investigated the chemical composition of rain water in the Amazon and found Cl^- concentrations being higher than Na^+ in places close to the Atlantic ocean, while the places located further away from the Atlantic coast presented a higher Na^+ than Cl^- concentration. The observed excess in Cl^- concentration at our study site compared to Na^+ means that there is a relevant influence from the Pacific ocean, indeed, despite the barrier effect of the Andes for the transport of air masses.

Through factor analysis it was possible to describe how sodium and chloride are related to the other elements measured and thus, to identify if common pathways are present that could give us hints on the possible origin of sodium and chloride. To conclude from contributions to the first two components, sea-salt represented by sodium and chloride had a strong relevance in both, rain and OP. Two likely origins could be approximated depending on the location of sodium and chloride in the multidimensional space: east (presumably the Atlantic), when the sodium and chloride air mass history was shared with elements of Amazon biomass-burning emissions (nitrate and sulfate, as revealed by Boy et al., 2008; Fabian et al., 2005; Makowski Giannoni et al., 2013, 2014) and west (probably the Pacific Ocean), when sodium and chloride presented an individual and unique air mass history. The latter means that solely sodium and chloride load to a factor as depicted in Fig. 3. Considerng that, at Cerro del Consuelo MS rain was more associated with an Atlantic origin of sodium and chloride, and OP with a Pacific origin (Fig. 3a). At El Tiro MS it is the other way around, with sea-salt from rain having more a westward origin and that from OP more an eastward origin (Fig. 3b). Source partitioning by factor analysis also allowed to identify the effects of local winds and pollution in the lower elevations. The influence of chloride-containing dust blown from the Loja-Zamora road and biomass-burning plumes from local fires are the most likely cause of the high chloride concentration at the ECSF MS. Findings by Yokouchi et al. (2002), Spanos (2002), Hildemann et al. (1991), and Harrison and Pio (1983) substantiates this assumption. According to these studies chloride does not only stems from sea-spray but is also emitted from natural and anthropogenic terrestrial sources, namely dust, biomass-burnig and biogenic forest emissions. This can be inferred from the time-series and factor analysis (Figs. 2 and 3) too. The distribution of chloride and its relation to other ions are distinct between valley and the mountain tops, where the concentration in the former is influenced by local winds and emissions, while that in the latter depends most likely only from the synoptic air-mass transport and emissions from distant sources. Being a conservative ion, sodium has very few sources others than ocean spray. This property of sodium is reflected in the time series (Fig. 2), in that no influence of local sources could be noticed.

To determine the relevance of Pacific sources to the sea-salt transport into the study area, back-trajectories statistical analysis and PSCF and CWT were used. Three different height levels were considered for analyzing the pathways of air mass transport (see Figs. 4–7). On the basis of a cluster analysis, the trajectories could be grouped together and 6 dominant pathways were identified (C1–C6): 3 eastern pathways, coming from the Atlantic Ocean, and 3 with a western or north-western origin, originating from or passing over the Pacific. In general, at all evaluated height levels the eastern

ACPD
15, 27177–27218, 2015

clusters predominate in the frequency of occurrence (approx. 90 %), which indicates that most of the air masses arriving in the study area originates over the Atlantic. However, even though easterlies prevail, when linking the main transport pathways to the observed concentration at the study site (see Table 1) we notice that the easterly trajectories are dominant in terms of frequency of occurrence, but they do not have the greatest impact, considering that they only contribute to small sea-salt concentration. The reason is that the highest concentration is contributed by the Pacific sources in the west and partially by the north-easterlies. Consequently, though the Pacific transport is very sporadic in nature, it contributes to up to 25 % of the total concentration at the study area with respect to the analyzed time span between 2004 and 2009.

In order to relate the air mass transport to potential spatial sources of sea-salt the PSCF and CWT were examined. The results showed that both hypothesized source areas contribute to the highest concentration at the receptor site: these areas are the equatorial Pacific in the vicinity of the coast of Ecuador and northern Peru as well as the equatorial Atlantic and the Caribbean sea. Because of the vicinity of the Pacific Ocean, the transported aerosols have a lower probability to be scavenged as compared to the long-range transport from the Atlantic over the Amazon. This is most likely the reason why the sources in the Pacific appear stronger and contribute to the highest concentration at the receptor site. Comparisons between the selected height levels revealed similar results which point to comparable atmospheric circulation patterns at these altitudes. The best results were gained by the CWT model (Fig. 7g, h and i), in successfully allocating the source hot spots over the oceans, distinguishing the hot spots from moderately contribution areas which are sometimes terrestrial. On the contrary, the PSCF was less successful in identifying the areas that contributed to the highest concentration. As already pointed out by Hsu et al. (2003) and Stohl (1996) a drawback of the PSCF method is that the values slightly higher and much higher than a defined threshold get similar probabilities which complicates their distinction. Thus, the results of the PSCF were heavily influenced by the arbitrary choice of the threshold concentration. Pekney et al. (2006) reported that the election of the threshold value

ACPD
15, 27177–27218, 2015

relies on the evaluated concentration time-series. The authors stated that for low background values and high concentration peaks, the 90th percentile threshold performs better, while for concentration time-series with less variability, the 75th percentile is more appropriate. In our case, the quite strong variations in the sea-salt concentration with season explained why the PSCF with 90th percentile threshold performed better than the 75th percentile.

Finally, because the general atmospheric circulation and thus, the air mass transport over South America is characterized by a seasonal behaviour which is well documented by in several studies (e.g., Bendix and Lauer, 1992; Bendix et al., 2008a; Emck, 2007), its effects on the source areas identified by the hybrid receptor models and the clusters associated to these areas was tested (Figs. 8–10). Furthermore, seasonal patterns could be observed in the measured concentration, particularly at the most exposed *Cerro del Consuelo* MS, which highlights its consideration. The quite regular occurrence of the highest concentration between September and February (Fig. 3), is in good agreement to the cluster-concentration statistics and the potential sources defined by PSCF and CWT. The highest concentration at the receptor site were contributed during SON and DJF (see Fig. 10). This means that the largest quantities of sea-salt were transported within this period mainly occurring from the equatorial Pacific and Atlantic. The westerlies are most successful in this period because the ITCZ is located further South (Rollenbeck et al., 2011).

The analysis of seasonal patterns in the sea-salt transport strengthen the predominance of air mass transport by eastern trajectories. Moreover, it confirmed that the western trajectories had the strongest impact contributing to the highest sea-salt concentration, because the large quantities were added in a short period of time (only approx 10 % of trajectories), but contributed up to 25 % of the total concentration (see Table 1) during the analyzed period. That means, despite the barrier effect of the Andes and the low frequency of occurrence of western pathways, the Pacific sea-salt sources play a relevant role in contributing to sea-salt transport to our study site. The comparison of the sodium and chloride concentration measured at our area of investigation

ACPD
15, 27177–27218, 2015

with that in other sites located further east substantiates the important role of the Pacific sources at our study area (Table 2). Even if the concentration in South Ecuador was not that high as observed in forests close to the Atlantic, despite the larger distance from the Atlantic coast it clearly exceeded the concentrations measured in the central Brazilian Amazon thousands of kilometers to the east.

6 Conclusions

We have used back-trajectory statistical analysis and source-receptor models to assess the allocation and contribution of Pacific and Atlantic Ocean sources to sea-salt (sodium and chloride) concentration to our study area in the Andes of South-East Ecuador. As input parameter to the back-trajectory analysis we integrated MACC reanalysis sea-salt concentration. As hypothesized, both Atlantic and Pacific sources play an important role to the transport of sea-salt to the study area in south-eastern Ecuador at the eastern Andean slopes. The greatest impact was produced by the equatorial Pacific and Atlantic sources and was seasonally driven with the greatest contributions taking place in austral late spring (SON) and summer (DJF) when the ITCZ migrates further South. In total, the Pacific sources only, contributed to up to 25 % of the total concentration at the study site, which represents an important addition to the total atmospheric sea-salt transport into our study site. Along the examined altitudinal gradient, a difference was observed in terms of the temporal variability of the concentration and its level where the highest and more exposed evaluated station presented a stronger seasonality linked to the large scale circulation. These seasonal patterns were observed in the MACC concentration data as well. The lowermost station was influenced by the mountain-valley winds and the local aerosols transported. Additionally, the higher chloride than sodium concentration and the higher concentration observed at our site in comparison to areas in the central Brazilian Amazon stresses the important role played by the Pacific sources regarding sea-salt transport.

ACPD
15, 27177–27218, 2015

Acknowledgements. We thank the German Academic Exchange Service (DAAD) for funding the PhD thesis of S. Makowski Giannoni (Ref. no. A/08/98222) and the German Research Foundation (DFG) for the funding of the work in the scope of the Research Unit RU816 (funding no. BE 1780/15-1). We are grateful to Giulia F. Curatola Fernández and Tim Appelhans for their valuable help. We also thank the foundation Nature & Culture International (NCI) Loja and San Diego for logistic support.

References

Beck, E., Bendix, J., Kottke, I., Makeschin, F., and Mosandl, R., eds.: Gradients in a tropical mountain ecosystem of Ecuador, vol. 198 of Ecological Studies, Springer Berlin/Heidelberg, Berlin, Germany, doi:10.1007/978-3-540-73526-7, 2008. 27181

Bendix, J. and Lauer, W.: Die Niederschlagsjahreszeiten in Ecuador und ihre klimadynamische Interpretation, Erdkunde, 46 pp., 1992. 27196

Bendix, J., Rollenbeck, R., and Reudenbach, C.: Diurnal patterns of rainfall in a tropical Andean valley of southern Ecuador as seen by a vertically pointing K–band Doppler radar, Int. J. Climatol., 26, 829–846, doi:10.1002/joc.1267, 2006. 27182

Bendix, J., Rollenbeck, R., Goettlicher, D., Nauss, T., and Fabian, P.: Seasonality and diurnal pattern of very low clouds in a deeply incised valley of the eastern tropical Andes (South Ecuador) as observed by a cost–effective WebCam system, Meteorol. Appl., 15, 281–291, doi:10.1002/met.72, 2008a. 27182, 27189, 27191, 27196

Bendix, J., Rollenbeck, R., Richter, M., Fabian, P., and Emck, P.: Climate, in: Gradients in a Tropical Mountain Ecosystem of Ecuador, edited by Beck, E., Bendix, J., Kottke, I., Makeschin, F., and Mosandl, R., , Springer Berlin/Heidelberg, ecological edn., chap. 1, 63–74, doi:10.1007/978-3-540-73526-7_8, 2008b. 27182

Bendix, J., Beck, E., Brauning, A., Makeschin, F., Mosandl, R., Scheu, S., and Wilcke, W., eds.: Ecosystem services, biodiversity and environmental change in a tropical mountain ecosystem of South Ecuador, vol. 221, Springer, Berlin-Heidelberg, doi:10.1007/978-3-642-38137-9, 2013. 27181

Bobbink, R., Hicks, K., and Galloway, J.: Global assessment of nitrogen deposition effects on terrestrial plant diversity: a synthesis, Ecol. Appl., 20, 30–59, doi:10.1890/08-1140.1, 2010. 27179

Boy, J., Rollenbeck, R., Valarezo, C., and Wilcke, W.: Amazonian biomass burning-derived acid and nutrient deposition in the north Andean montane forest of Ecuador, Global Biogeochem. Cy., 22, GB4011, doi:10.1029/2007GB003158, 2008. 27194

Brookshire, E. N. J., Hedin, L. O., Newbold, J. D., Sigman, D. M., and Jackson, J. K.: Sustained losses of bioavailable nitrogen from montane tropical forests, Nat. Geosci., 5, 123–126, doi:10.1038/ngeo1372, 2012. 27179

Carslaw, D. C. and Ropkins, K.: openair – An R package for air quality data analysis, Environ. Model. Softw., 27-28, 52–61, doi:10.1016/j.envsoft.2011.09.008, 2012. 27184

Dentener, F., Drevet, J., Lamarque, J. F., Bey, I., Eickhout, B., Fiore, a. M., Hauglustaine, D., Horowitz, L. W., Krol, M., Kulshrestha, U. C., Lawrence, M., Galy-Lacaux, C., Rast, S., Shindell, D., Stevenson, D., Van Noije, T., Atherton, C., Bell, N., Bergman, D., Butler, T., Cofala, J., Collins, B., Doherty, R., Ellingsen, K., Galloway, J., Gauss, M., Montanaro, V., Müller, J. F., Pitari, G., Rodriguez, J., Sanderson, M., Solmon, F., Strahan, S., Schultz, M., Sudo, K., Szopa, S., and Wild, O.: Nitrogen and sulfur deposition on regional and global scales: A multimodel evaluation, Global Biogeochem. Cy., 20, GB4003, doi:10.1029/2005GB002672, 2006. 27179

Draxler, R. and Hess, G.: An overview of the HYSPLIT_4 modeling system of trajectories, dispersion, and deposition, Australian Meteorological Magazine, 47, 295–308, 1998. 27184

Dudley, R., Kaspari, M., and Yanoviak, S. P.: Lust for Salt in the Western Amazon, Biotropica, 44, 6–9, doi:10.1111/j.1744-7429.2011.00818.x, 2012. 27179, 27180

Emck, P.: A climatology of South Ecuador, Phd thesis, University of Erlangen, http://www.opus.ub.uni-erlangen.de/opus/volltexte/2007/656/ (last access: 2 October 2015), 2007. 27182, 27189, 27191, 27196

Fabian, P., Kohlpaintner, M., and Rollenbeck, R.: Biomass burning in the Amazon-fertilizer for the mountaineous rain forest in Ecuador, Environ. Sci. Pollut. Res., 12, 290–296, 2005. 27194

Fabian, P., Rollenbeck, R., Spichtinger, N., Brothers, L., Dominguez, G., and Thiemens, M.: Sahara dust, ocean spray, volcanoes, biomass burning: pathways of nutrients into Andean rainforests, Adv. Geosci., 22, 85–94, doi:10.5194/adgeo-22-85-2009, 2009. 27180

Fleming, Z. L., Monks, P. S., and Manning, A. J.: Review: Untangling the influence of air-mass history in interpreting observed atmospheric composition, Atmos. Res., 104-105, 1–39, doi:10.1016/j.atmosres.2011.09.009, 2012. 27185

ACPD
15, 27177–27218, 2015

Forti, M. C., Melfi, A. J., Astolfo, R., and Fostier, A.-H.: Rainfall chemistry composition in two ecosystems in the northeastern Brazilian Amazon (Amapá State), J. Geophys. Res., 105, 28895, doi:10.1029/2000JD900235, 2000. 27207

Galloway, J. N., Townsend, A. R., Erisman, J. W., Bekunda, M., Cai, Z., Freney, J. R., Martinelli, L. a., Seitzinger, S. P., and Sutton, M. a.: Transformation of the nitrogen cycle: recent trends, questions, and potential solutions, Science (New York, N.Y.), 320, 889–92, doi:10.1126/science.1136674, 2008. 27179

Griffith, K. T., Ponette-González, A. G., Curran, L. M., and Weathers, K. C.: Assessing the influence of topography and canopy structure on Douglas fir throughfall with LiDAR and empirical data in the Santa Cruz mountains, USA, Environ. Monit. Assess., 187, 4486, doi:10.1007/s10661-015-4486-6, 2015. 27181

Guelle, W., Schulz, M., Balkanski, Y., and Dentener, F.: Influence of the source formulation on modeling the atmospheric global distribution of sea salt aerosol, J. Geophys. Res., 106, 27509, doi:10.1029/2001JD900249, 2001. 27184

Harrison, R. M. and Pio, C. A.: Major ion composition and chemical associations of inorganic atmospheric aerosols., Environ. Sci. Technol., 17, 169–74, doi:10.1021/es00109a009, 1983. 27194

Hildemann, L. M., Markowski, G. R., and Cass, G. R.: Chemical composition of emissions from urban sources of fine organic aerosol, Environ. Sci. Technol., 25, 744–759, doi:10.1021/es00016a021, 1991. 27194

Homeier, J., Hertel, D., Camenzind, T., Cumbicus, N. L., Maraun, M., Martinson, G. O., Poma, L. N., Rillig, M. C., Sandmann, D., Scheu, S., Veldkamp, E., Wilcke, W., Wullaert, H., and Leuschner, C.: Tropical andean forests are highly susceptible to nutrient inputs-rapid effects of experimental N and p addition to an ecuadorian montane forest., PloS one, 7, e47128, doi:10.1371/journal.pone.0047128, 2012. 27179

Hsu, Y.-K., Holsen, T. M., and Hopke, P. K.: Comparison of hybrid receptor models to locate PCB sources in Chicago, Atmos. Environ., 37, 545–562, doi:10.1016/S1352-2310(02)00886-5, 2003. 27185, 27195

Jaeglé, L., Quinn, P. K., Bates, T. S., Alexander, B., and Lin, J.-T.: Global distribution of sea salt aerosols: new constraints from in situ and remote sensing observations, Atmos. Chem. Phys., 11, 3137–3157, doi:10.5194/acp-11-3137-2011, 2011. 27183

Kalnay, E., Kanamitsu, M., Kistler, R., Collins, W., Deaven, D., Gandin, L., Iredell, M., Saha, S., White, G., Woollen, J., et al.: The NCEP/NCAR 40-year reanalysis project, B. Am. Meteorol. Soc., 77, 437–471, 1996. 27184

Kaspari, M., Yanoviak, S. P., and Dudley, R.: On the biogeography of salt limitation: a study of ant communities., P. Natl. Acad. Sci. USA, 105, 17848–17851, doi:10.1073/pnas.0804528105, 2008. 27179, 27180

Kaspari, M., Yanoviak, S. P., Dudley, R., Yuan, M., and Clay, N. A.: Sodium shortage as a constraint on the carbon cycle in an inland tropical rainforest., P. Natl. Acad. Sci. USA, 106, 19405–19409, doi:10.1073/pnas.0906448106, 2009. 27179

Keene, W. C., Pszenny, A. A. P., Galloway, J. N., and Hawley, M. E.: Sea-salt corrections and interpretation of constituent ratios in marine precipitation, J. Geophys. Res., 91, 6647, doi:10.1029/JD091iD06p06647, 1986. 27183

Kirchner, M., Fegg, W., Römmelt, H., Leuchner, M., Ries, L., Zimmermann, R., Michalke, B., Wallasch, M., Maguhn, J., Faus-Kessler, T., and Jakobi, G.: Nitrogen deposition along differently exposed slopes in the Bavarian Alps, Sci. Total Environ., 470-471, 895–906, doi:10.1016/j.scitotenv.2013.10.036, 2014. 27181

Koehler, B., Corre, M. D., Veldkamp, E., Wullaert, H., and Wright, S. J.: Immediate and long-term nitrogen oxide emissions from tropical forest soils exposed to elevated nitrogen input, Glob. Change Biol., 15, 2049–2066, doi:10.1111/j.1365-2486.2008.01826.x, 2009. 27179

Lee, A. T. K., Kumar, S., Brightsmith, D. J., and Marsden, S. J.: Parrot claylick distribution in South America: do patterns of “where” help answer the question “why”?, Ecography, 33, 503–513, doi:10.1111/j.1600-0587.2009.05878.x, 2009. 27180

Lizcano, D. J. and Cavelier, J.: Características Químicas de salados y hábitos alimenticios de la Danta de montaña (Tapirus pinchaque Roulin, 1829) en los Andes Centrales de Colombia, Mastozoología neotropical, 11, 193–201, 2004. 27180

Lovett, G. and Kinsman, J.: Atmospheric pollutant deposition to high-elevation ecosystems, Atmos. Environ.-A. Gen., 24, 2767–2786, 1990. 27181

Makowski Giannoni, S., Rollenbeck, R., Fabian, P., and Bendix, J.: Complex topography influences atmospheric nitrate deposition in a neotropical mountain rainforest, Atmos. Environ., 79, 385–394, doi:10.1016/j.atmosenv.2013.06.023, 2013. 27181, 27194

Makowski Giannoni, S., Rollenbeck, R., Trachte, K., and Bendix, J.: Natural or anthropogenic? On the origin of atmospheric sulfate deposition in the Andes of southeastern Ecuador, Atmos. Chem. Phys., 14, 11297–11312, doi:10.5194/acp-14-11297-2014, 2014. 27194

ACPD

15, 27177–27218, 2015

Atmospheric deposition of sea-salt in South-eastern Ecuador

S. Makowski Giannoni et al.

Matson, A. L., Corre, M. D., and Veldkamp, E.: Nitrogen cycling in canopy soils of tropical montane forests responds rapidly to indirect N and P fertilization., Glob. Change Biol., 20, 3802–13, doi:10.1111/gcb.12668, 2014. 27179

Millero, F.: Treatise on Geochemistry, Elsevier, doi:10.1016/B978-0-08-095975-7.00601-X, 2014. 27183

Morcrette, J.-J., Boucher, O., Jones, L., Salmond, D., Bechtold, P., Beljaars, a., Benedetti, a., Bonet, a., Kaiser, J. W., Razinger, M., Schulz, M., Serrar, S., Simmons, a. J., Sofiev, M., Suttie, M., Tompkins, a. M., and Untch, a.: Aerosol analysis and forecast in the European Centre for Medium-Range Weather Forecasts Integrated Forecast System: Forward modeling, J. Geophys. Res., 114, D06206, doi:10.1029/2008JD011235, 2009. 27184

Pauliquevis, T., Lara, L. L., Antunes, M. L., and Artaxo, P.: Aerosol and precipitation chemistry measurements in a remote site in Central Amazonia: the role of biogenic contribution, Atmos. Chem. Phys., 12, 4987–5015, doi:10.5194/acp-12-4987-2012, 2012. 27207

Pekney, N. J., Davidson, C. I., Zhou, L., and Hopke, P. K.: Application of PSCF and CPF to PMF-Modeled Sources of PM 2.5 in Pittsburgh, Aerosol Sci. Technol., 40, 952–961, doi:10.1080/02786820500543324, 2006. 27185, 27195

Pett-Ridge, J. C.: Contributions of dust to phosphorus cycling in tropical forests of the Luquillo Mountains, Puerto Rico, Biogeochemistry, 94, 63–80, doi:10.1007/s10533-009-9308-x, 2009. 27179

Phoenix, G. K., Hicks, K. W., Cinderby, S., Kuylenstierna, J. C. I., Stock, W. D., Dentener, F. J., Giller, K. E., Austin, A. T., Lefroy, R. D. B., Gimeno, B. S., Ashmore, M. R., and Ineson, P.: Atmospheric nitrogen deposition in world biodiversity hotspots: the need for a greater global perspective in assessing N deposition impacts, Glob. Change Biol., 12, 470–476, doi:10.1111/j.1365-2486.2006.01104.x, 2006. 27179

Powell, L. L., Powell, T. U., Powell, G. V. N., and Brightsmith, D. J.: Parrots Take it with a Grain of Salt: Available Sodium Content May Drive Collpa (Clay Lick) Selection in Southeastern Peru, Biotropica, 41, 279–282, doi:10.1111/j.1744-7429.2009.00514.x, 2009. 27179, 27180, 27185

Pozzer, A., de Meij, A., Pringle, K. J., Tost, H., Doering, U. M., van Aardenne, J., and Lelieveld, J.: Distributions and regional budgets of aerosols and their precursors simulated with the EMAC chemistry-climate model, Atmos. Chem. Phys., 12, 961–987, doi:10.5194/acp-12-961-2012, 2012. 27183

Richter, M., Beck, E., Rollenbeck, R., and Bendix, J.: The study area, in: Ecosystemservices, biodiversity and environmental change in a tropical mountain ecosystem of South Ecuador, edited by Bendix, J., Beck, E., Brauning, A., Makeschin, F., Mosandl, R., Scheu, S., and Wilcke, W., chap. 1, Springer Berlin/Heidelberg, Berlin, Germany, doi:10.1007/978-3-642-38137-9_1, 2013. 27182

Riuttanen, L., Hulkkonen, M., Dal Maso, M., Junninen, H., and Kulmala, M.: Trajectory analysis of atmospheric transport of fine particles, SO_2, NO_x and O_3 to the SMEAR II station in Finland in 1996–2008, Atmos. Chem. Phys., 13, 2153–2164, doi:10.5194/acp-13-2153-2013, 2013. 27185

Robinson, N. H., Newton, H. M., Allan, J. D., Irwin, M., Hamilton, J. F., Flynn, M., Bower, K. N., Williams, P. I., Mills, G., Reeves, C. E., McFiggans, G., and Coe, H.: Source attribution of Bornean air masses by back trajectory analysis during the OP3 project, Atmos. Chem. Phys., 11, 9605–9630, doi:10.5194/acp-11-9605-2011, 2011. 27185

Rollenbeck, R., Bendix, J., Fabian, P., Boy, J., Wilcke, W., Dalitz, H., Oesker, M., and Emck, P.: Comparison of different techniques for the measurement of precipitation in tropical montane rain forest regions, J. Atmos. Ocean. Technol., 24, 156–168, doi:10.1175/JTECH1970.1, 2007. 27183

Rollenbeck, R., Bendix, J., and Fabian, P.: Spatial and temporal dynamics of atmospheric water inputs in tropical mountain forests of South Ecuador, Hydrol. Process., 25, 344–352, doi:10.1002/hyp.7799, 2011. 27182, 27183, 27196

Schemenauer, R. S. and Cereceda, P.: A proposed standard fog collector for use in high-elevation regions, J. Appl. Meteorol., 33, 1313–1322, 1994. 27183

Schulz, M., de Leeuw, G., and Balkanski, Y.: Sea-salt aerosol source functions and emissions, in: Emissions of Atmospheric Trace Compounds, 333–359, Springer Netherlands, doi:10.1007/978-1-4020-2167-1_9,, 2004. 27184

Seibert, P., Kromb-Kolb, H., Baltensperger, U., Jost, D., and Schwikowski, M.: Trajectory analysis of high-alpine air pollution data, in: NATO challenges of modern society, edited by Gryning, S.-E. and Millán, M. M., pp. 595–596, Springer US, doi:10.1007/978-1-4615-1817-4_65, 1994. 27186

Spanos, T.: Environmetric modeling of emission sources for dry and wet precipitation from an urban area, Talanta, 58, 367–375, doi:10.1016/S0039-9140(02)00285-0, 2002. 27194

Stohl, A.: Trajectory statistics-A new method to establish source-receptor relationships of air pollutants and its application to the transport of particulate sulfate in Europe, Atmos. Environ., 30, 579–587, doi:10.1016/1352-2310(95)00314-2, 1996. 27195
Tanner, E. V. J., Vitousek, P. M., and Cuevas, E.: Experimental investigation of nutrient limitation of forest growth on wet tropical mountains, Ecology, 79, 10–22, doi:10.1890/0012-9658(1998)079[0010:EIONLO]2.0.CO;2, 1998. 27179
Tardy, Y., Bustillo, V., Roquin, C., Mortatti, J., and Victoria, R.: The Amazon. Biogeochemistry applied to river basin management, Appl. Geochem. 20, 1746–1829, doi:10.1016/j.apgeochem.2005.06.001, 2005. 27180, 27183, 27193, 27207
Vet, R., Artz, R. S., Carou, S., Shaw, M., Ro, C.-U., Aas, W., Baker, A., Bowersox, V. C., Dentener, F., Galy-Lacaux, C., Hou, A., Pienaar, J. J., Gillett, R., Forti, M. C., Gromov, S., Hara, H., Khodzher, T., Mahowald, N. M., Nickovic, S., Rao, P., and Reid, N. W.: A global assessment of precipitation chemistry and deposition of sulfur, nitrogen, sea salt, base cations, organic acids, acidity and pH, and phosphorus, Atmos. Environ., 93, 3–100, doi:10.1016/j.atmosenv.2013.10.060, 2014. 27183
Vitousek, P. M.: Litterfall, Nutrient Cycling, and Nutrient Limitation in Tropical Forests, 65, 285–298, 1984. 27179
Voigt, C. C., Capps, K. A., Dechmann, D. K. N., Michener, R. H., and Kunz, T. H.: Nutrition or detoxification: why bats visit mineral licks of the Amazonian rainforest., PloS one, 3, e2011, doi:10.1371/journal.pone.0002011, 2008. 27179, 27180
Wang, F., Li, J., Wang, X., Zhang, W., Zou, B., Neher, D. A., and Li, Z.: Nitrogen and phosphorus addition impact soil N2O emission in a secondary tropical forest of South China., Scientific reports, 4, 5615, doi:10.1038/srep05615, 2014. 27179
Wilcke, W., Leimer, S., Peters, T., Emck, P., Rollenbeck, R., Trachte, K., Valarezo, C., and Bendix, J.: The nitrogen cycle of tropical montane forest in Ecuador turns inorganic under environmental change, Global Biogeochem. Cy., 27, 1194–1204, doi:10.1002/2012GB004471, 2013. 27179
Williams, M. R., Fisher, T. R., and Melack, J. M.: Chemical composition and deposition of rain in the central Amazon, Brazil, Atmos. Environ., 31, 207–217, doi:10.1016/1352-2310(96)00166-5, 1997. 27207
Wolf, K., Veldkamp, E., Homeier, J., and Martinson, G. O.: Nitrogen availability links forest productivity, soil nitrous oxide and nitric oxide fluxes of a tropical montane forest in southern Ecuador, Global Biogeochem. Cy., 25, GB4009, doi:10.1029/2010GB003876, 2011. 27179

Wullaert, H., Geographie, P., Chemie, F., and Gutenberg-universit, J.: Response of nutrient cycles of an old-growth montane forest in Ecuador to experimental low-level nutrient amendments, Ph.D. thesis, http://ubm.opus.hbz-nrw.de/volltexte/2010/2312/, 2010. 27179

Yokouchi, Y., Ikeda, M., Inuzuka, Y., and Yukawa, T.: Strong emission of methyl chloride from tropical plants, Nature, 416, 163–5, doi:10.1038/416163a, 2002. 27194

Yu, H., Chin, M., Yuan, T., Bian, H., Remer, L. A., Prospero, J. M., Omar, A., Winker, D., Yang, Y., Zhang, Y., Zhang, Z., and Zhao, C.: The Fertilizing Role of African Dust in the Amazon Rainforest: A First Multiyear Assessment Based on CALIPSO Lidar Observations, Geophys. Res. Lett., 42, 1984–1991, doi:10.1002/2015GL063040, 2015. 27179

Zeng, Y. and Hopke, P.: A study of the sources of acid precipitation in Ontario, Canada, Atmos. Environ., 23, 1499–1509, doi:10.1016/0004-6981(89)90409-5, 1989. 27185

ACPD
15, 27177–27218, 2015

Table 1. Mean sea-salt concentration and percentage of total concentration at the receptor site in the Andes of south-eastern Ecuador associated to each mean trajectory cluster (C1–C6) for the considered height levels. The percentage contribution of the mean clusters to the total concentration is shown in parenthesis.

	Mean sea-salt concentration ($kg\,kg^{-1}$) and relative total concentration (%)		
	3180 m	4200 m	6000 m
C1	1.33E-09 (30.32)	1.41E-09 (28.39)	7.53E-10 (30.93)
C2	6.68E-10 (22.83)	7.57E-10 (24.81)	8.36E-10 (23.76)
C3	1.93E-09 (8.53)	6.46E-10 (24.48)	1.49E-09 (7.44)
C4	2.40E-09 (7.97)	2.07E-09 (8.08)	2.16E-09 (11.86)
C5	2.01E-09 (9.17)	2.37E-09 (6.60)	1.17E-09 (26.02)
C6	6.67E-10 (21.18)	1.96E-09 (7.65)	1.79E-09 (5.68)

ACPD
15, 27177–27218, 2015

Table 2. Comparison of the Na^+ and Cl^- mean concentration in precipitation in this study with data from other sites in the Amazon basin. The values represent Volume Weighted Means expressed in $\mu eq\,L^{-1}$.

	Na^+	Cl^-	Reference
South Ecuador (RBSF)	7.80	9.60	This study
Central Amazon (Manaus)	7.78	7.70	Tardy et al. (2005)
Central Amazon (Lake Calado)	2.40	4.60	Williams et al. (1997)
Central Amazon (Balbina)	3.80	5.20	Pauliquevis et al. (2012)
Northeast Amazon	16.60	16.90	Forti et al. (2000)
Eastern Amazon (Belem)	18.90	19.50	Tardy et al. (2005)

ACPD
15, 27177–27218, 2015

Table A1. Results from the correlation analysis between sea-salt monthly mean concentration from MACC reanalysis data and Na^+ and Cl^- monthly mean concentration from El Tiro and Cerro del Consuelo meteorological station (MS) samples. Correlation was tested for the different height levels of the MACC data set.

	MACC1 (0.03–0.5 µm)			MACC2 (0.5–5 µm)			MACC3 (5–20 µm)		
	Cl^-	Na^+	mean	Cl^-	Na^+	mean	Cl^-	Na^+	mean
Cerro del Consuelo									
700 hPa	0.36**	0.35**	0.18	0.52***	0.52***	0.40***	0.48***	0.47***	0.52***
600 hPa	0.31**	0.26*	0.1	0.50***	0.47***	0.39**	0.36**	0.30*	0.40***
500 hPa	0.27*	0.19	0.03	0.47***	0.36**	0.30*	0.22	0.13	0.28*
400 hPa	0.24*	0.19	0.03	0.37**	0.27*	0.23	0.08	0.02	0.17
300 hPa	0.11	0.02	−0.05	0.25*	0.16	0.23	0.01	−0.05	0.14
200 hPa	0.22	0.09	0.03	0.30*	0.18	0.25*	−0.02	−0.04	0.08
El Tiro									
700 hPa	0.34**	0.18	0.18	0.41***	0.17	0.2	0.32**	0.05	0.16
600 hPa	0.37**	0.22	0.2	0.40***	0.14	0.18	0.19	−0.08	0.07
500 hPa	0.33**	0.18	0.16	0.31**	0.05	0.09	0.02	−0.15	−0.04
400 hPa	0.24*	0.14	0.12	0.14	−0.02	0	−0.14	−0.16	−0.12
300 hPa	0.14	0.15	0.1	−0.01	−0.08	−0.05	−0.21	−0.15	−0.13
200 hPa	0.15	0.15	0.19	−0.01	−0.12	0.01	−0.17	0.01	−0.04

Note: * $p < 0.05$, ** $p < 0.01$, *** $p < 0.001$.

ACPD
15, 27177–27218, 2015

Atmospheric deposition of sea-salt in South-eastern Ecuador

S. Makowski Giannoni et al.

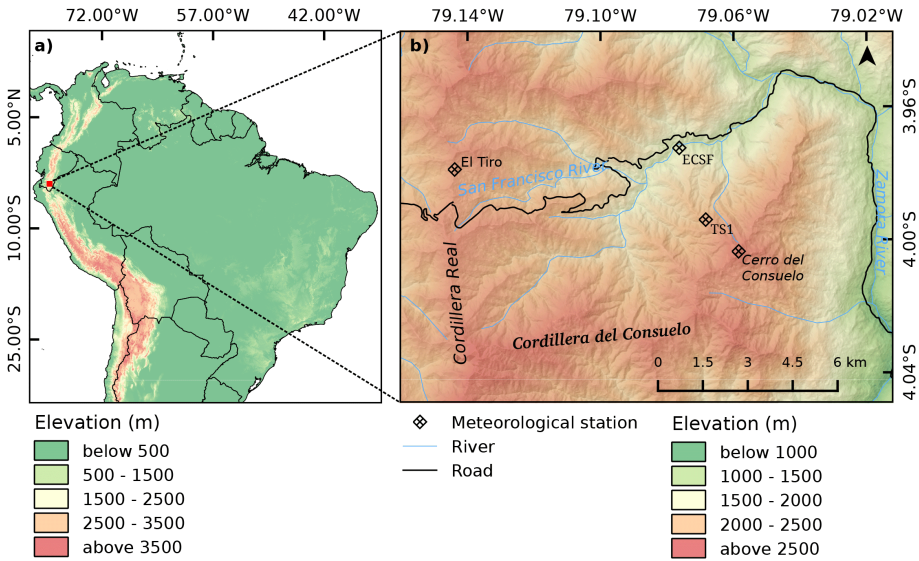

Figure 1. Map of the study area. **(a)** Location of the study area in the Huancabamba depression of the Andes in South-America. **(b)** Detailed map of the rain and occult precipitation (OP) sampling sites installed in the study area.

ACPD
15, 27177–27218, 2015

Atmospheric deposition of sea-salt in South-eastern Ecuador

S. Makowski Giannoni et al.

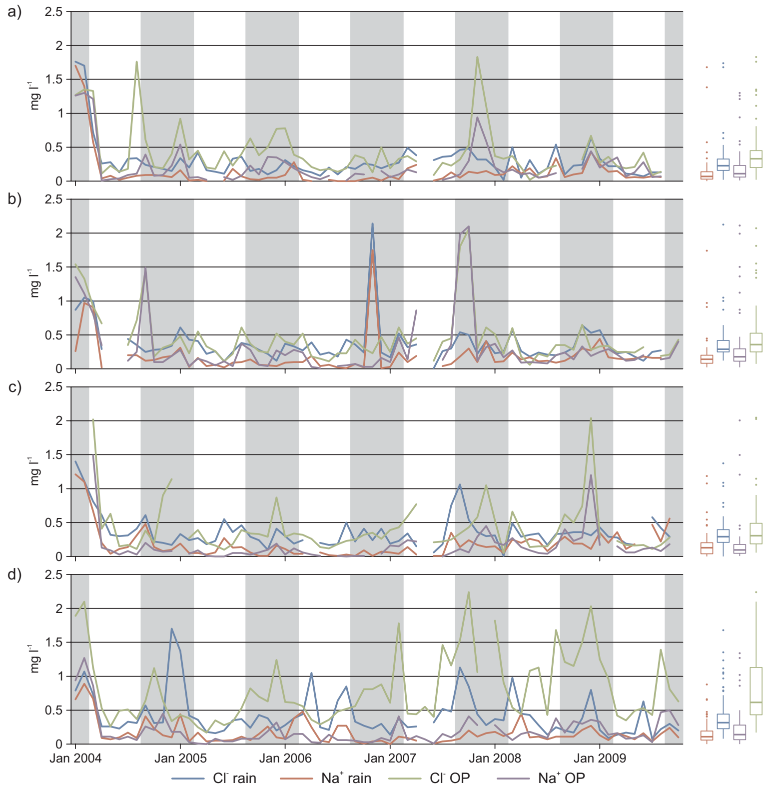

Figure 2. Time-series of Na^+ and Cl^- volume weighted monthly mean (VWMM) concentration in rain and occult precipitation (OP) samples from meteorological stations (MSs) at different altitudes and topographical locations: **(a)** Cerro del Consuelo (3180 m), **(b)** El Tiro (2825 m), **(c)** TS1 (2660 m), and **(d)** ECSF (1960 m). The shaded areas cover 6 months periods from September to February. The box plots on the right column show the distribution of each time-series. The boxes symbolize the lower and upper quartile of the data. Vertical lines show ranges of observed concentration and points are outliers.

ACPD
15, 27177–27218, 2015

Atmospheric deposition of sea-salt in South-eastern Ecuador

S. Makowski Giannoni et al.

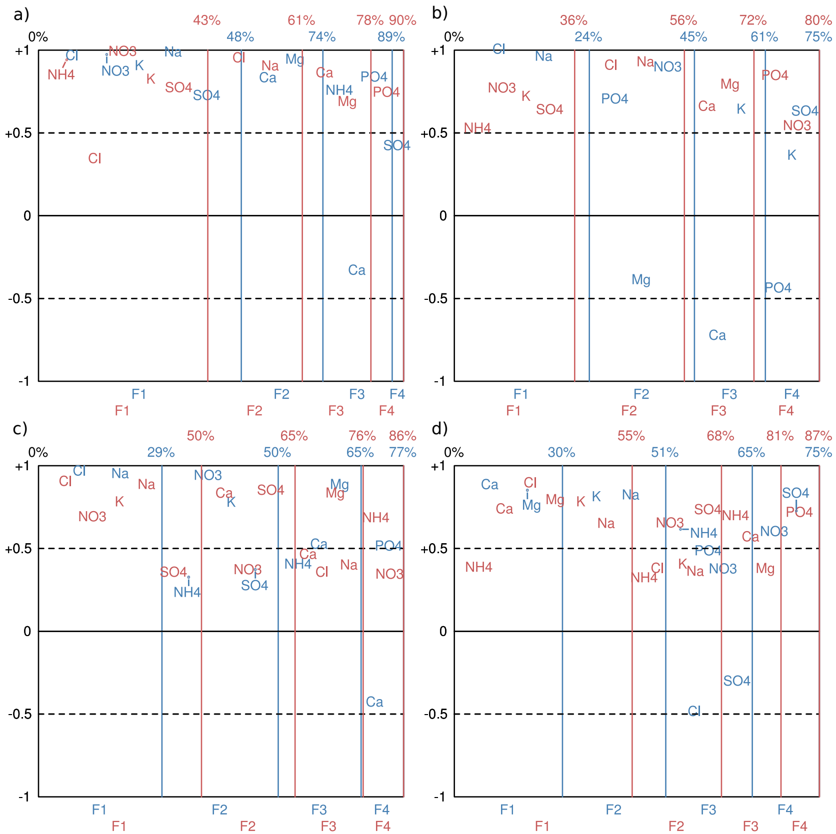

Figure 3. Factor analysis with varimax rotation of major ions in rain (in blue) and occult precipitation (OP, in red) samples from **(a)** Cerro del Consuelo, **(b)** El Tiro, **(c)** TS1, and **(d)** ECSF meteorological stations (MSs). The bottom *x* axis represents the resulting factors; the upper *x* axis shows the explained variability; and the *y* axis represents the loadings.

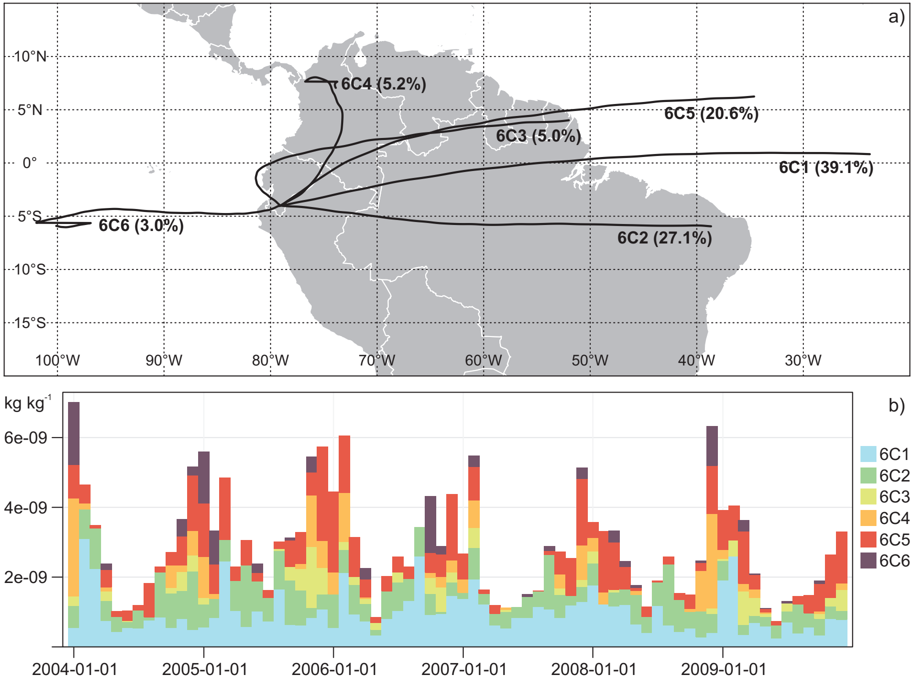

Figure 4. (a) Mean back-trajectories at 6000 m height level for the calculated clusters with origin at the San Francisco catchment in the Andes of south-eastern Ecuador and **(b)** monthly time-series of sea-salt concentration from MACC reanalysis shown by the contribution of each cluster to the concentration.

ACPD
15, 27177–27218, 2015

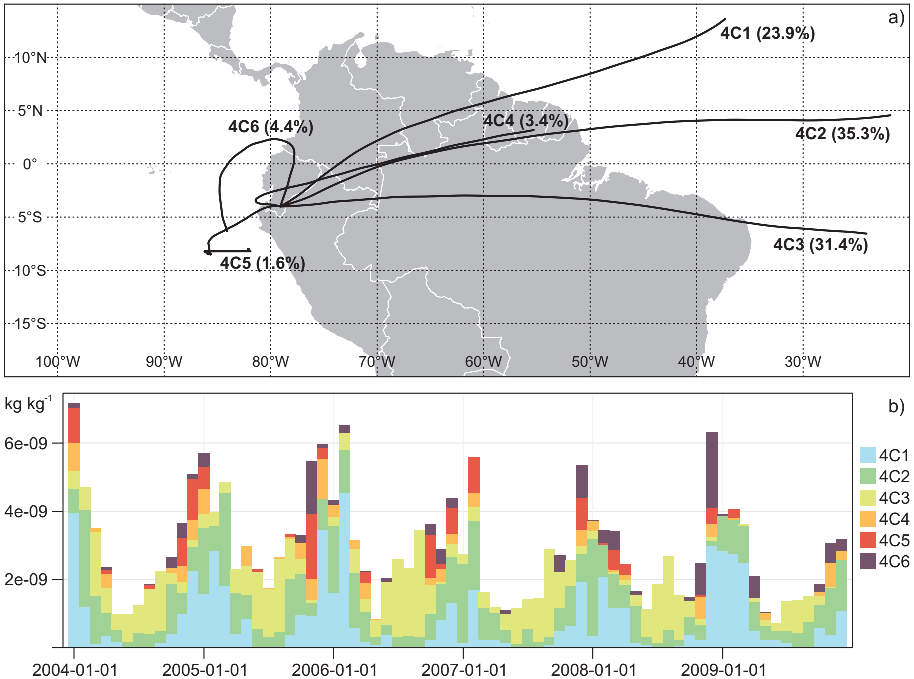

Figure 5. As Fig. 4 but for height level at 4200 m.

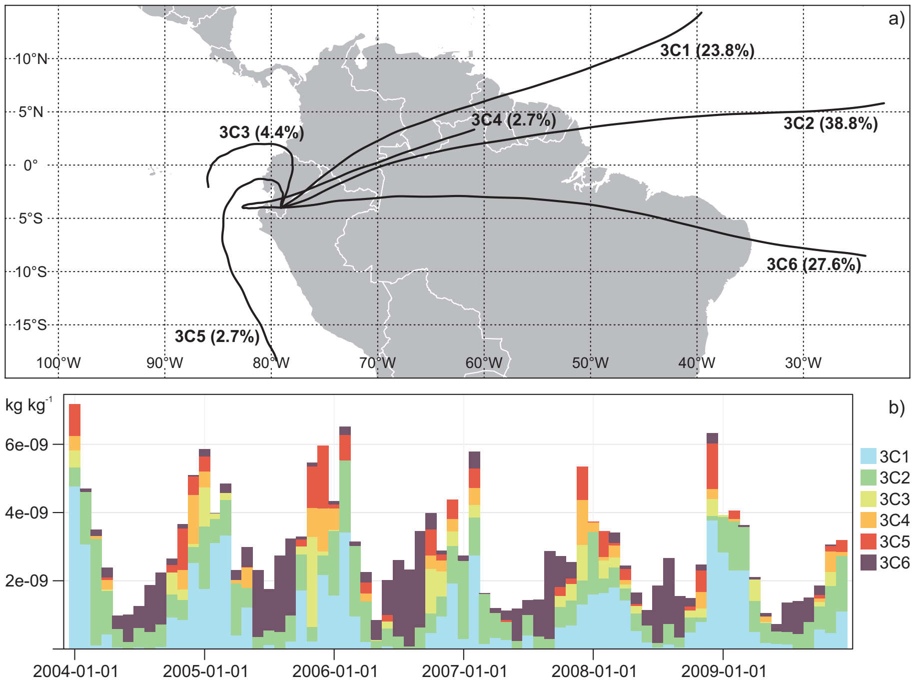

Figure 6. As Fig. 4 but for height level at 3180 m.

ACPD
15, 27177–27218, 2015

Atmospheric deposition of sea-salt in South-eastern Ecuador

S. Makowski Giannoni et al.

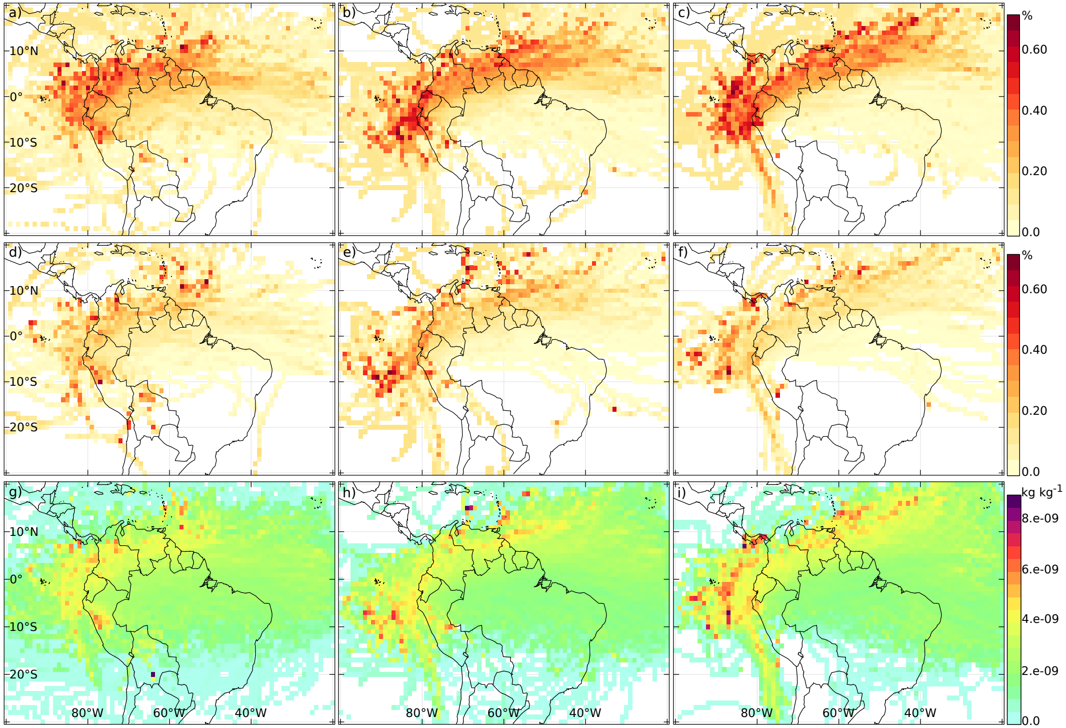

Figure 7. Potential source contribution function (PSCF) for **(a, b, c)** 75th and **(d, e, f)** 90th percentiles and **(g, h, i)** concentration weighted trajectory (CWT) maps for the 2004–2009 period and three different trajectory arrival height levels: 6000 m (left column), 4200 m (middle column), and 3180 m (right column).

ACPD
15, 27177–27218, 2015

Atmospheric deposition of sea-salt in South-eastern Ecuador

S. Makowski Giannoni et al.

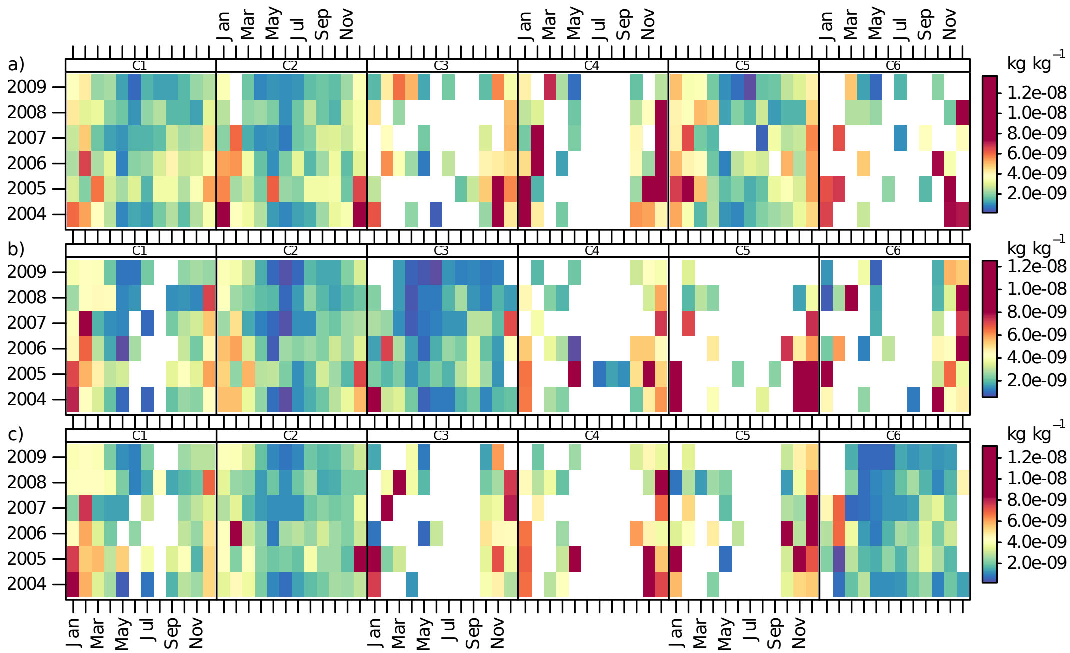

Figure 8. Sea salt concentration plotted by month (x axis) and year (y axis), and by cluster number for **(a)** 6000 m, **(b)** 4200 m, and **(c)** 3180 m height level.

ACPD
15, 27177–27218, 2015

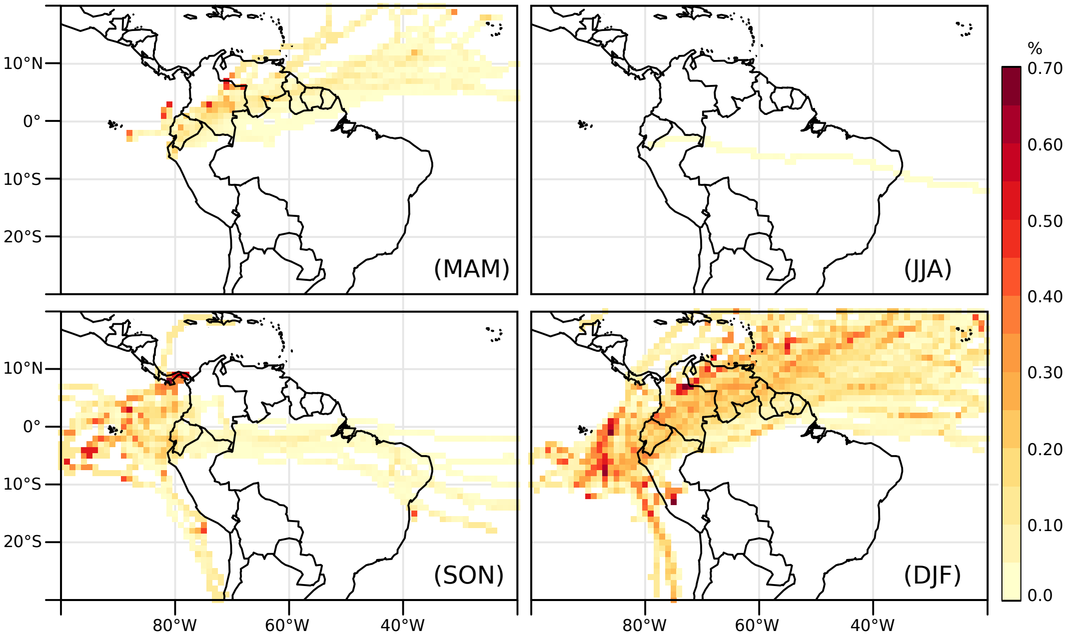

Figure 9. Maps of seasonal potential source contribution function (PSCF), 90th percentile concentration; trajectory arrival height level is 3180 m.

ACPD
15, 27177–27218, 2015

Atmospheric deposition of sea-salt in South-eastern Ecuador

S. Makowski Giannoni et al.

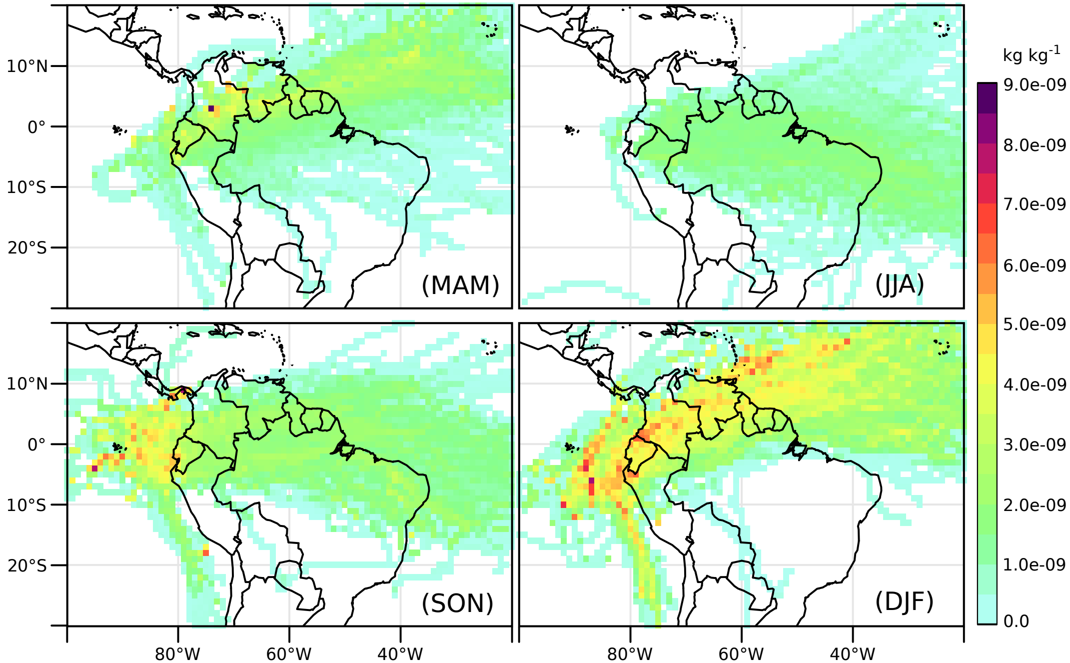

Figure 10. As Fig. 9 but for concentration weighted trajectory (CWT).

ACPD
15, 27177–27218, 2015

Atmospheric deposition of sea-salt in South-eastern Ecuador

S. Makowski Giannoni et al.

Title Page
Abstract | Introduction
Conclusions | References
Tables | Figures
◀| |▶
◀ ▶
Back | Close
Full Screen / Esc
Printer-friendly Version
Interactive Discussion